Probing compressed mass spectra in the type-II seesaw model at the LHC

Saiyad Ashanujjaman[1,2,*] and Siddharth P. Maharathy[3,4,†]

[1]*Department of Physics, SGTB Khalsa College, Delhi 110007, India*
[2]*Department of Physics and Astrophysics, University of Delhi, Delhi 110007, India*
[3]*Institute of Physics, Bhubaneswar, Sachivalaya Marg, Sainik School, Bhubaneswar 751005, India*
[4]*Homi Bhabha National Institute, Training School Complex, Anushakti Nagar, Mumbai 400094, India*

(Received 15 May 2023; accepted 6 June 2023; published 21 June 2023)

Despite a great deal of effort in searching for the tripletlike Higgses in the type-II seesaw model, evidence for their production is yet to be found at the LHC. As such, one might be in the balance regarding this model's relevance at the electroweak scale. In this work, we peruse a scenario, akin to compressed mass spectra in supersymmetry, which might have eluded the experimental searches thus far. We perform a multivariate analysis to distinguish signals with a pair of same-sign leptons with low invariant mass from the Standard Model processes, including those accruing from *fake* leptons and electron charge misidentification, and find that a significant part of the hitherto unconstrained parameter space could be probed with the already collected run 2 13 TeV LHC and future HL-LHC data.

DOI: 10.1103/PhysRevD.107.115026

I. INTRODUCTION

The type-II seesaw model [1–6], extending the Standard Model (SM) with an $SU(2)_L$ triplet scalar field with hypercharge $Y = 1$, offers a tenable explanation for the observed neutrino masses and mixings; as such, it is arguably the most widely studied neutrino mass model [7–70]. This model accommodates, in addition to the 125 GeV Higgs, several other physical states: doubly charged scalar ($H^{\pm\pm}$), singly charged scalar ($H^{\pm}$), and CP-even and CP-odd neutral scalars (H^0 and A^0). The phenomenology of these states, particularly $H^{\pm\pm}$, has been studied extensively at the Large Hadron Collider (LHC) [7–47], electron colliders [48–56], muon colliders [57–60], and electron-proton colliders [61,62]; see Refs. [44,63,64] for comprehensive reviews. Experimental collaborations have performed several searches for $H^{\pm\pm}$ [71–82], and nonobservations of any significant excess over the SM expectations have led to stringent limits on them. While the ATLAS Collaboration has set a lower limit of 1020 GeV for $H^{\pm\pm}$ decaying into $\ell^{\pm}\ell^{\pm}$ (with $\ell = e, \mu$) [82], the CMS Collaboration has set a lower limit of 535 GeV for those decaying into $\tau^{\pm}\tau^{\pm}$ [76]. For $H^{\pm\pm}$ decaying into $W^{\pm}W^{\pm}$, the ATLAS Collaboration has excluded them within the mass range 200–350 GeV [81].

Recently, Ref. [44] has estimated exclusion limits on $m_{H^{\pm\pm}}$ for a vast model parameter space, characterized by the mass splitting $\Delta m = m_{H^{\pm\pm}} - m_{H^{\pm}}$ and the triplet vacuum expectation value (VEV) v_t, by recasting several searches performed by the CMS and ATLAS Collaborations.[1] The regions corresponding to $\Delta m = 0$ and $\Delta m < 0$, being dominated with the so-called "golden decays" of $H^{\pm\pm}$ to $\ell^{\pm}\ell^{\pm}$ and $W^{\pm}W^{\pm}$, are highly constrained by the LHC searches, as such $H^{\pm\pm}$ up to 1115 (420) GeV masses are excluded for small (large) v_t. On the other hand, a significantly large part of the model parameter space characterized by $\Delta m \sim \mathcal{O}(10)$ GeV and $v_t \sim \mathcal{O}(10^{-7})$–$\mathcal{O}(10^{-3})$ is largely unconstrained by the existing LHC searches. A detailed analysis for probing this region at future e^-e^+ colliders has been performed in Ref. [55]. This region is dominated by the exclusive decays to one or more off-shell $W^{\pm}$ bosons and H^0/A^0. While the latter decays to $\nu\nu$ for $v_t \leq \mathcal{O}(10^{-4})$ and to $b\bar{b}, t\bar{t}, ZZ, Zh, hh$ for $v_t \geq \mathcal{O}(10^{-4})$, the former results in leptons and jets with relatively low transverse momentum (p_T), termed as soft leptons and soft jets.

The present work concerns part of the above-mentioned unconstrained region where H^0/A^0 exclusively decays to $\nu\nu$. Therefore, the resulting final state is populated with soft leptons and jets and low missing transverse momentum

*saiyad.a@iopb.res.in
†siddharth.m@iopb.res.in

[1]For $H^{\pm\pm}$ decaying into $W^{\pm}W^{\pm}$, Ref. [44] estimates an improved exclusion range of 200–400 GeV compared to 200–350 GeV obtained by the ATLAS Collaboration in Ref. [81].

(p_T^{miss}). Typically, these are beset with oversized background contributions from quantum chromodynamics (QCD) multijet, multitop, and Drell-Yan processes and, thus, are not highly sensitive to new physics searches. Such signals, akin to those appearing in compressed mass spectra in supersymmetry, in principle, can be distinguished from the SM background by requiring either a jet with large p_T from initial state radiation that leads to a high boost of the decaying particle pair and, thus, large p_T^{miss} [83,84] or two or more soft leptons along with large p_T^{miss} [85,86]. However, as it turns out, the requirement of an energetic jet or large p_T^{miss} exceedingly reduces the signal rate, thereby making such searches insensitive to the present model [44]. Keeping this in mind, we relax the aforementioned requirement to retain signal acceptance and require only a pair of same-sign leptons with low invariant mass. We perform a multivariate analysis to distinguish such characteristic signal from the SM background, including those arising from *fake* leptons and electron charge misidentification.

The rest of this work is structured as follows. We briefly outline the type-II seesaw model in Sec. II, followed by a detailed collider analysis in Sec. III and a summary in Sec. IV.

II. THE HIGGS TRIPLET

In addition to the SM field content, the type-II seesaw model employs an $SU(2)_L$ triplet scalar field with $Y = 1$:

$$\Delta = \begin{pmatrix} \Delta^+/\sqrt{2} & \Delta^{++} \\ \Delta^0 & -\Delta^+/\sqrt{2} \end{pmatrix}.$$

The scalar potential involving Δ and the SM Higgs doublet $\Phi = (\,\Phi^+ \quad \Phi^0\,)^T$ is given by [67]

$$\begin{aligned} V(\Phi,\Delta) = &-m_\Phi^2 \Phi^\dagger\Phi + \frac{\lambda}{4}(\Phi^\dagger\Phi)^2 + m_\Delta^2 \mathrm{Tr}(\Delta^\dagger\Delta) \\ &+ [\mu(\Phi^T i\sigma^2 \Delta^\dagger \Phi) + \mathrm{H.c.}] + \lambda_1(\Phi^\dagger\Phi)\mathrm{Tr}(\Delta^\dagger\Delta) \\ &+ \lambda_2[\mathrm{Tr}(\Delta^\dagger\Delta)]^2 + \lambda_3 \mathrm{Tr}[(\Delta^\dagger\Delta)^2] + \lambda_4 \Phi^\dagger \Delta\Delta^\dagger \Phi, \end{aligned}$$

where m_Φ^2, m_Δ^2, and μ are the mass parameters and λ and λ_i ($i = 1, \ldots, 4$) are the dimensionless quartic couplings. The neutral components Φ^0 and Δ^0 procure respective VEVs v_d and v_t such that $\sqrt{v_d^2 + 2v_t^2} = 246$ GeV. For a detailed description of the main dynamical features of the scalar potential, see Ref. [67]. After the electroweak symmetry breaking, mixing of the identically charged states results in several physical states:

(i) Φ^0 and Δ^0 mix into two CP-even states (h and H^0) and two CP-odd states (G^0 and A^0);
(ii) $\Phi^\pm$ and $\Delta^\pm$ mix into two mass states $G^\pm$ and $H^\pm$;
(iii) $\Delta^{\pm\pm}$ is aligned with its mass state $H^{\pm\pm}$.

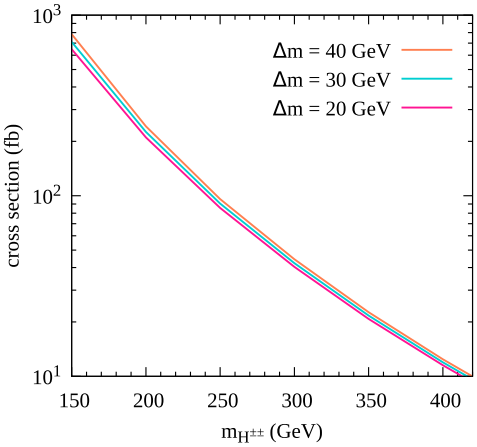

FIG. 1. LO total cross section for $pp \to H^{++}H^{--}$ and $pp \to H^{\pm\pm}H^{\mp}$ for $\Delta m = 20$, 30, and 40 GeV.

G^0 and $G^\pm$ are the *would-be* Nambu-Goldstone bosons, h is identified as the 125 GeV Higgs observed at the LHC, and the rest follows the sum rule

$$m_{H^{\pm\pm}}^2 - m_{H^\pm}^2 \approx m_{H^\pm}^2 - m_{H^0/A^0}^2 \approx -\frac{\lambda_4}{4} v_d^2.$$

The Yukawa interaction $Y_{ij}^\nu L_i^T C i\sigma^2 \Delta L_j$ (L_i stands for the SM lepton doublet, with $i \in e, \mu, \tau$, and C the charge-conjugation operator) induces masses for the neutrinos:

$$m_\nu = \sqrt{2} Y^\nu v_t.$$

The tripletlike Higgses are pair produced at the LHC via the neutral and charged current Drell-Yan mechanisms[2]:

$$\begin{aligned} q\bar{q} &\to \gamma^*/Z^* \to H^{++}H^{--}, H^+H^-, H^0A^0, \\ qq' &\to W^{\pm *} \to H^{\pm\pm}H^\mp, H^\pm H^0, H^\pm A^0. \end{aligned}$$

We evaluate the leading-order (LO) cross sections using the SARAH 4.14.4 [87,88] generated UFO [89] modules in MadGraph5_aMC_v2.7.3 [90,91] with the NNPDF23_LO_AS_0130_QED parton distribution function [92,93]. Figure 1 shows the LO total production cross section for $pp \to H^{++}H^{--}$ and $pp \to H^{\pm\pm}H^\mp$ at the 13 TeV LHC as a function of $m_{H^{\pm\pm}}$ for $\Delta m = 20$, 30, and 40 GeV. For brevity, we do not include the other processes, as they do not contribute to the final state considered in Sec. III. Following the QCD corrections estimated in Ref. [94], we naively scale the LO cross section by a next-to-leading-order (NLO) K factor of 1.15.

[2]They are also produced via t/u-channel photon fusion as well as vector-boson fusion processes. However, such processes are rather subdominant.

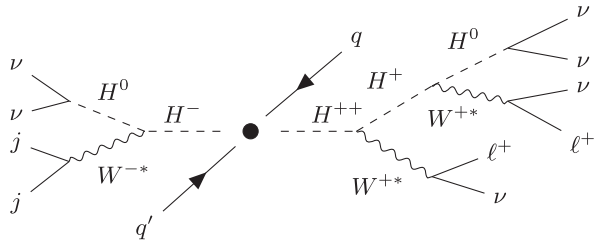

FIG. 2. Schematic diagram for $qq' \to H^{++}H^-$ leading to a pair of same-sign leptons and p_T^{miss} in the final state.

III. COLLIDER ANALYSIS

In broad terms, the phenomenology of this model depends on three parameters, namely, $m_{H^{\pm\pm}}$, v_t, and $\Delta m = m_{H^{\pm\pm}} - m_{H^{\pm}}$; see Refs. [16,20,44] for detailed discussions. As mentioned earlier, the present work concerns the unconstrained parameters space characterized by $\Delta m \sim \mathcal{O}(10)$ GeV and $v_t \lesssim \mathcal{O}(10^{-4})$, where $H^{\pm\pm}$ and $H^{\pm}$ exclusively decay into off-shell $W^{\pm}$ bosons and H^0/A^0, with the latter further decaying into $\nu\nu$.[3] Therefore, the resulting final state is populated with soft leptons and jets and low p_T^{miss}. A pair of same-sign leptons constitute the final state signature of the search presented in this work; see Fig. 2.

In the following, we briefly outline the relevant SM background processes, the selection of various physics objects, and event selection and then perform a multivariate analysis to distinguish the signal from background.

A. SM backgrounds

The final state with a pair of same-sign leptons is beset with fewer SM background contributions compared to other final states with leptons and jets. However, for the present analysis, we consider numerous SM processes such as diboson, triboson, and tetraboson processes, Higgsstrahlung processes, single and multitop productions in association with or without gauge bosons, and Drell-Yan processes. All these processes are generated using MadGraph5_aMC_v2.7.3 [90,91] at the LO precision in perturbative QCD, with the *MLM merging* scheme to consolidate additional partons using PYTHIA 8.2 [95], and then naively scaled by appropriate NLO (or higher, whichever is available in the literature) K factors [91,96–110].

The relevant backgrounds can be broadly divided into three categories.

(i) *Prompt background.*—Particles originating from (very close vicinity of) the primary interaction point constitute this background, with the dominant contributions coming from the diboson and top-pair production processes.

(ii) *Nonprompt and fake background.*—Processes where a jet is misidentified as a lepton or additional leptons originate from initial and final state radiation (ISR and FSR, respectively) photon conversions and in-flight heavy-flavor decays constitute this background. Though the lepton isolation requirements (mentioned in Sec. III B) significantly subdue this contribution, a considerable fraction passes the object selection. Estimating this contribution requires a data-driven approach, the so-called *fake factor* method, which is beyond the scope of this work. We adopt a conservative approach, assuming a p_T-dependent probability of 0.1%–0.3% for a jet to be misidentified as a lepton [111].

(iii) *Electron charge misidentification.*—Bremsstrahlung interaction of the electrons with the inner detector material triggering trident events and sniff tracks could lead to charge misidentification. Therefore, a small fraction of prompt background events with a pair of opposite-sign leptons (mainly from Drell-Yan and top-pair production processes) can lead to same-sign leptons in the final states. To account for this effect, all prompt electrons are naively corrected with a p_T- and η-dependent charge misidentification probability: $P(p_T, \eta) = \sigma(p_T) \times f(\eta)$, where $\sigma(p_T)$ and $f(\eta)$ ranges from 0.02 to 0.1 and 0.03 to 1, respectively [112].

B. Object selection

We pass the MadGraph5_aMC_v2.7.3 generated parton-level events into PYTHIA 8.2 [95] to simulate subsequent decays for the unstable particles, ISR and FSR, showering, fragmentation and hadronization and then into DELPHES 3.4.2 with the default CMS card [113] for simulating detector effects as well as reconstructing various physics objects, viz. photons, electrons, muons, and jets.

The jet constituents are clustered using the anti-k_T *algorithm* [114] with a jet radius $R = 0.4$ as implemented in FastJet 3.3.2 [115]. While the jets are required to be within the pseudorapidity range $|\eta| < 2.4$ and have a transverse momentum $p_T > 20$ GeV, the leptons (electrons and muons) are required to have $|\eta| < 2.5$ and $p_T > 10$ GeV. Furthermore, to ensure that the leptons are isolated, we demand the scalar sum of the p_T's of all other objects lying within a cone of radius 0.3 (0.4) around an electron (a muon) to be smaller than 10% (15%) of its p_T. Finally, p_T^{miss} is estimated from the momentum imbalance in the transverse direction associated to all reconstructed objects (including photons) in an event.

C. Event selection

The present analysis requires events with a pair of same-sign isolated leptons. For such events, we apply the following preselection requirements.

[3]The analysis presented in this work is largely insensitive to the value of v_t as long as $v_t \lesssim \mathcal{O}(10^{-4})$; thus, we do not commit to a fixed value for v_t.

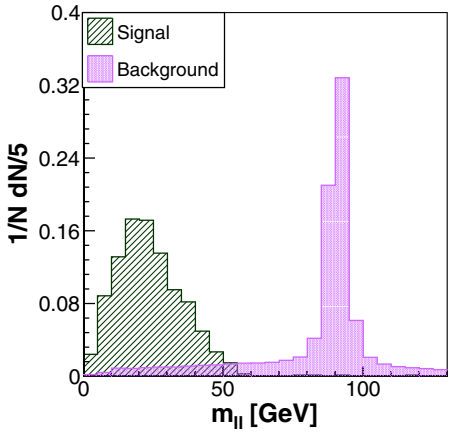

FIG. 3. Normalized distributions of $m_{\ell\ell}$ for the signal (BP1) and background events after the $p_T(\ell_{1,2}) > 15$ GeV selection.

(i) We reject events with $m_{\ell\ell} \in [3, 3.2]$ GeV to lessen the contribution from J/ψ resonance. No veto is applied around other resonances like Υ or Ψ, as these contributions are rather subdominant.
(ii) We require $m_{\ell\ell} > 1$ GeV and the angular separation between the leptons $\Delta R_{\ell\ell} > 0.05$ to suppress the nearly collinear lepton pairs resulting from ISR and FSR photon conversions or spurious pairs of tracks with shared hits from muon bremsstrahlung interactions.
(iii) Leptons are required to separated from the reconstructed jets by $\Delta R_{\ell,j} > 0.4$. This, along with the lepton isolation requirements, suppresses nonprompt leptons from in-flight heavy-flavor decays.
(iv) Both the leptons are required to have $p_T > 15$ GeV. Though this is at par with the dilepton triggers used in 2015 in the run 2 LHC [116], a little higher p_T thresholds have been used [117,118] in the later years. A trigger with higher p_T thresholds would reduce the signal acceptance. Therefore, to retain the signal rate, a "combined" trigger with $p_T(\ell_{1,2}) > 15$ GeV and the dilepton invariant mass $m_{\ell\ell} < 60$ GeV can be used.

Shown in Fig. 3 are the normalized distributions of $m_{\ell\ell}$ for the signal and background events after the $p_T(\ell_{1,2}) > 15$ GeV selection. The signal events are shown for a benchmark defined by

$$\text{BP1}: m_{H^{\pm\pm}} = 200 \text{ GeV}, \qquad \Delta m = 30 \text{ GeV}.$$

For the signal, it falls rapidly with an end point near 60 GeV as occasioned by the compressed mass spectrum considered in BP1. On the contrary, the background boasts a peak at the Z-boson mass with the lion's share of the contributions accruing from $Z \to e^- e^+$ due to electron charge misidentification. Not only does the selection $m_{\ell\ell} < 60$ GeV help with the trigger, but it also vanquishes the oversized background contribution.

TABLE I. Summary of optimized BDT hyperparameters.

BDT hyperparameter	Optimized choice
NTrees	500
MinNodeSize	5%
MaxDepth	5
BoostType	AdaBoost
AdaBoostBeta	0.1
UseBaggedBoost	True
BaggedSampleFraction	0.5
SeparationType	GiniIndex
nCuts	20

D. Multivariate analysis

We now perform a multivariate analysis with the boosted decision tree (BDT) classifier implemented in the TMVA 4.3 toolkit [119] integrated into ROOT 6.24 [120] to distinguish the signals from backgrounds. For training and testing the classifier, 10^6 signal events for each $m_{H^{\pm\pm}}$ within the [150,400] GeV range in steps of 50 GeV and at least of worth 3000 fb^{-1} luminosity of background events are fed. Of these, 50% are picked randomly for training, and the rest are used for testing. The classifier is trained with the *adaptive boost* algorithm with a learning rate of 0.1, 500 decision trees with 5% minimum node size, and a depth of five layers per tree into a forest, and the *Gini index* is used for node splitting. The relevant BDT hyperparameters are summarized in Table I.

We use the following kinematic variables as input features to the BDT classifier[4]:

$$p_T(\ell_{1,2}), \qquad p_T^{\text{miss}}, \qquad m_{\ell\ell}, \qquad \Delta R_{\ell\ell}, \qquad \frac{p_T(\ell\ell)}{L_T} \quad \text{and} \quad \Delta\phi(\ell\ell, p_T^{\text{miss}}),$$

where $p_T(\ell\ell)$ is the dilepton system's p_T and L_T is the scalar sum of all jets and leptons' p_T. Normalized distributions for some of these features are shown in Fig. 4; the rest are not shown for brevity. These features constitute a minimal set with a good separation power between the signal and background, which is usually measured in terms of the method-unspecific separation and method-specific ranking. For a given feature x, the former is defined as

$$\langle S^2 \rangle = \frac{1}{2} \int \frac{[\hat{x}_S(x) - \hat{x}_B(x)]^2}{\hat{x}_S(x) + \hat{x}_B(x)} dx,$$

where $\hat{x}_S(x)$ and $\hat{x}_B(x)$ are the probability density functions of x for the signal and background, respectively. The method-specific ranking demonstrates the relative

[4]Just like $\Delta R_{\ell\ell}$, the azimuthal separation between the leptons $\Delta\phi_{\ell\ell}$ can be used as an input feature. However, these two variables are highly correlated; thus, we drop the latter.

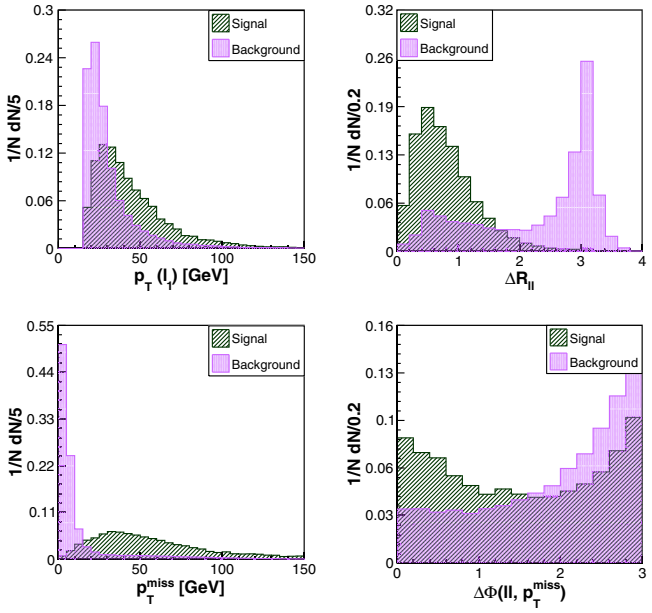

FIG. 4. Normalized distributions for some of the input features. The signal distributions are for BP1.

importance of the input features in separating the signal from background. Both these measures are shown in Table II. As it turns out, $\Delta R_{\ell\ell}$ is the best separating variable, while $p_T(\ell_{1,2})$ are the ones with least separating power. Shown in Fig. 5 is the Pearson linear correlation matrix, with the coefficients defined as

$$\rho(x,y) = \frac{\langle xy\rangle - \langle x\rangle\langle y\rangle}{\sigma_x \sigma_y},$$

where $\langle x\rangle$ and σ_x, respectively, are the expectation value and standard deviation of x. These input features are not highly correlated and, thus, constitute a minimal set. Lastly, the classifier is checked for overtraining by performing the Kolmogorov-Smirnov test which compares the BDT response curves for the training and testing subsamples. The response curves shown in Fig. 6 exhibit no considerable overtraining.

TABLE II. Method-unspecific separation and method-specific ranking of the input features.

Feature	Method-unspecific separation	Method-specific ranking
$p_T^{\rm miss}$	0.5945	0.214
$\Delta R_{\ell\ell}$	0.4777	0.3015
$\frac{p_T(\ell\ell)}{L_T}$	0.4586	0.2086
$m_{\ell\ell}$	0.368	0.08534
$p_T(\ell_1)$	0.1481	0.04751
$p_T(\ell_2)$	0.08474	0.05806
$\Delta\phi(\ell\ell, p_T^{\rm miss})$	0.03997	0.08499

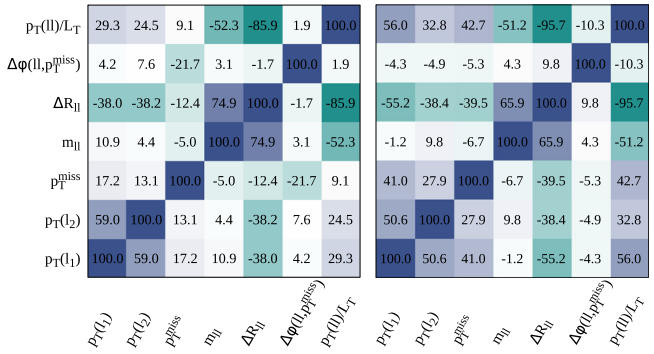

FIG. 5. Correlations in percent among the input features for the signal (left) and background (right).

For brevity, the receiver-operator-characteristic curve quantifying the BDT performance is not shown. Instead, we show the variation of the discovery significance (estimated using the formula given in Sec. III E) as a function of the BDT response for $m_{H^{\pm\pm}} = 200$, 300, and 400 GeV with $\Delta m = 30$ GeV in Fig. 7. As apparent from this, the discovery significance reaches its maximum for the BDT response of 0.4, albeit irrespective of $m_{H^{\pm\pm}}$, demonstrating the robustness of the BDT classifier's training. Therefore, to maximize the sensitivity of the search, we require

$$\text{BDTresponse} > 0.4.$$

Table III shows the remaining background and signal (for $m_{H^{\pm\pm}} = 200$, 300, and 400 GeV with $\Delta m = 30$ GeV) cross sections after the above selection.

E. Discovery and exclusion projection

Finally, we estimate the discovery and exclusion projection for different $m_{H^{\pm\pm}}$. The median expected discovery and exclusion significances are estimated as [121–123]

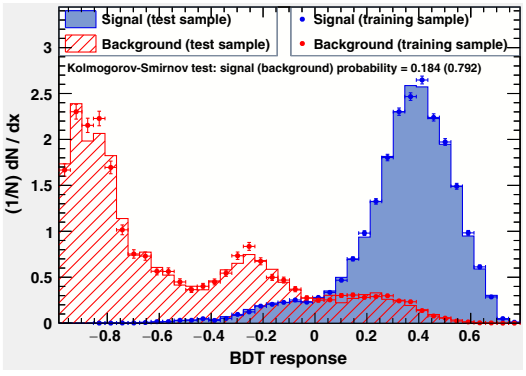

FIG. 6. BDT response curves for the training and testing subsamples.

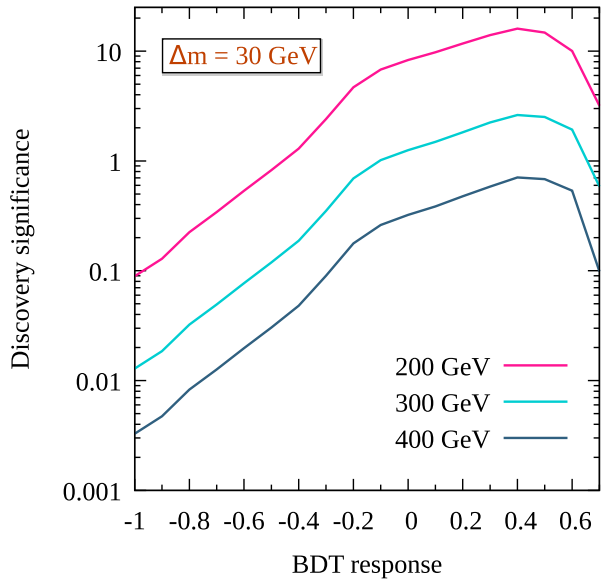

FIG. 7. Discovery significance as a function of the BDT response for $m_{H^{\pm\pm}} = 200$, 300, and 400 GeV with $\Delta m = 30$ GeV.

$$Z_{\rm dis} = \left[2\left((s+b)\ln\left[\frac{(s+b)(b+\delta_b^2)}{b^2+(s+b)\delta_b^2}\right] - \frac{b^2}{\delta_b^2}\ln\left[1+\frac{\delta_b^2 s}{b(b+\delta_b^2)}\right]\right)\right]^{1/2},$$

$$Z_{\rm exc} = \left[2\left\{s - b\ln\left(\frac{b+s+x}{2b}\right) - \frac{b^2}{\delta_b^2}\ln\left(\frac{b-s+x}{2b}\right)\right\} - (b+s-x)(1+b/\delta_b^2)\right]^{1/2},$$

where $x = \sqrt{(s+b)^2 - 4sb\delta_b^2/(b+\delta_b^2)}$, s and b are the numbers of signal and background events, respectively, and δ_b is the background uncertainty. Without going into the intricacy of estimating the latter, we assume it to be 20%, albeit conservatively. In Fig. 8, we show the required luminosities (in fb^{-1}) needed to achieve 95% confidence limits (C.L.) (1.645σ) exclusion and 5σ discovery as a function of $m_{H^{\pm\pm}}$ for $\Delta m = 20$, 30, and 40 GeV. For high $m_{H^{\pm\pm}}$, the signal cross section falls quickly and, thus, the sensitivity.

We find that, for $\Delta m = 30$ GeV, this model could be probed up to $m_{H^{\pm\pm}} = 260(330)$ GeV with 5σ discovery (95% C.L. exclusion) significance with the already collected run 2 LHC data (∼139 fb^{-1}), whereas, for the high-luminosity LHC (HL-LHC) with 3000 fb^{-1} data, this limit extends to 360 (420) GeV. For a smaller or larger Δm

TABLE III. Background and signal cross sections (fb) after the selection: BDT response > 0.4.

Event sample	Cross section (fb)
γ^*/Z^*	2.6344
$W^\pm Z$	1.4435
$W^\pm W^\pm V$ ($V = W, Z$)	0.7913
$t\bar{t}V$	0.7313
$t\bar{t}$	0.5535
Others	1.0618
Total background	7.2158
Signal: $(m_{H^{\pm\pm}}, \Delta m) = (200, 30)$ GeV	4.6235
Signal: $(m_{H^{\pm\pm}}, \Delta m) = (300, 30)$ GeV	0.6906
Signal: $(m_{H^{\pm\pm}}, \Delta m) = (400, 30)$ GeV	0.1841

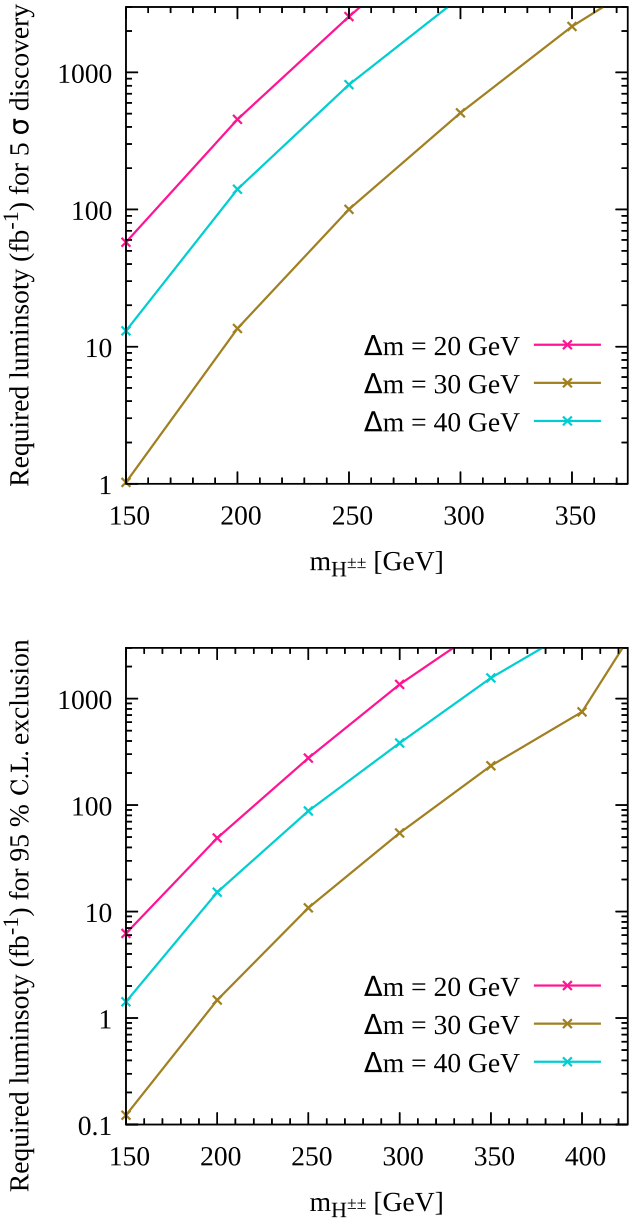

FIG. 8. Required luminosity (fb^{-1}) for 5σ discovery and 95% C.L. exclusion as a function of $m_{H^{\pm\pm}}$ for $\Delta m = 20$, 30, and 40 GeV.

(say, 20 or 40 GeV), the discovery and exclusion reaches are lower compared to those for $\Delta m = 30$ GeV. Understandably, the BDT classifier, being trained with signals with $\Delta m = 30$ GeV, is not maximally sensitive to other Δm. In addition, for smaller Δm, a significantly large fraction of the leptons emanating from the off-shell W bosons fail to pass the dilepton trigger requirements in Sec. III C, and, thus, the sensitivity is lower.

IV. SUMMARY

Nonobservations of any significant excess over the SM expectation in all the experimental searches looking for doubly charged Higgses thus far have led to stringent limits on them. While interpreted in the context of the type-II seesaw model, the tripletlike Higgses are already excluded up to a few hundred GeV masses for a vast region of the model parameter space [44]. In this work, we peruse a scenario, akin to compressed mass spectra in supersymmetry, which these experimental searches are not sensitive to and, consequently, is largely unconstrained. We perform a multivariate analysis to distinguish signals with a pair of same-sign leptons with low invariant mass from the SM processes, including those concerning fake leptons and electron charge misidentification, and find that a significant part of the hitherto unconstrained parameter space could be probed with the already collected run 2 LHC and future HL-LHC data.

In closing, we mention that the search strategy presented here is also applicable to other scalar extensions of the SM with compressed mass spectra where the lightest scalar state decays invisibly.

ACKNOWLEDGMENTS

S. A. acknowledges support from the SERB Core Research Grant No. CRG/2018/004889. The simulations were supported in part by the SAMKHYA: High Performance Computing Facility provided by Institute of Physics, Bhubaneswar.

[1] W. Konetschny and W. Kummer, Nonconservation of total lepton number with scalar bosons, Phys. Lett. **70B**, 433 (1977).
[2] T. P. Cheng and L.-F. Li, Neutrino masses, mixings and oscillations in $SU(2) \times U(1)$ models of electroweak interactions, Phys. Rev. D **22**, 2860 (1980).
[3] G. Lazarides, Q. Shafi, and C. Wetterich, Proton lifetime and fermion masses in an SO(10) model, Nucl. Phys. **B181**, 287 (1981).
[4] J. Schechter and J. W. F. Valle, Neutrino masses in $SU(2) \times U(1)$ theories, Phys. Rev. D **22**, 2227 (1980).
[5] R. N. Mohapatra and G. Senjanovic, Neutrino masses and mixings in gauge models with spontaneous parity violation, Phys. Rev. D **23**, 165 (1981).
[6] M. Magg and C. Wetterich, Neutrino mass problem and gauge hierarchy, Phys. Lett. **94B**, 61 (1980).
[7] K. Huitu, J. Maalampi, A. Pietila, and M. Raidal, Doubly charged Higgs at LHC, Nucl. Phys. **B487**, 27 (1997).
[8] J. F. Gunion, C. Loomis, and K. T. Pitts, Searching for doubly charged Higgs bosons at future colliders, eConf **C960625**, LTH096 (1996).
[9] S. Chakrabarti, D. Choudhury, R. M. Godbole, and B. Mukhopadhyaya, Observing doubly charged Higgs bosons in photon-photon collisions, Phys. Lett. B **434**, 347 (1998).
[10] M. Muhlleitner and M. Spira, A note on doubly charged Higgs pair production at hadron colliders, Phys. Rev. D **68**, 117701 (2003).
[11] A. G. Akeroyd and M. Aoki, Single and pair production of doubly charged Higgs bosons at hadron colliders, Phys. Rev. D **72**, 035011 (2005).
[12] A. G. Akeroyd, M. Aoki, and H. Sugiyama, Probing Majorana phases and neutrino mass spectrum in the Higgs triplet model at the CERN LHC, Phys. Rev. D **77**, 075010 (2008).
[13] J. Garayoa and T. Schwetz, Neutrino mass hierarchy and Majorana *CP* phases within the Higgs triplet model at the LHC, J. High Energy Phys. 03 (2008) 009.
[14] T. Han, B. Mukhopadhyaya, Z. Si, and K. Wang, Pair production of doubly-charged scalars: Neutrino mass constraints and signals at the LHC, Phys. Rev. D **76**, 075013 (2007).
[15] F. del Aguila and J. A. Aguilar-Saavedra, Distinguishing seesaw models at LHC with multi-lepton signals, Nucl. Phys. **B813**, 22 (2009).
[16] P. Fileviez Perez, T. Han, G.-y. Huang, T. Li, and K. Wang, Neutrino masses and the CERN LHC: Testing type II seesaw, Phys. Rev. D **78**, 015018 (2008).
[17] A. G. Akeroyd and C.-W. Chiang, Doubly charged Higgs bosons and three-lepton signatures in the Higgs triplet model, Phys. Rev. D **80**, 113010 (2009).
[18] A. G. Akeroyd, C.-W. Chiang, and N. Gaur, Leptonic signatures of doubly charged Higgs boson production at the LHC, J. High Energy Phys. 11 (2010) 005.
[19] A. Melfo, M. Nemevsek, F. Nesti, G. Senjanovic, and Y. Zhang, Type II seesaw at LHC: The roadmap, Phys. Rev. D **85**, 055018 (2012).
[20] M. Aoki, S. Kanemura, and K. Yagyu, Testing the Higgs triplet model with the mass difference at the LHC, Phys. Rev. D **85**, 055007 (2012).
[21] A. G. Akeroyd and H. Sugiyama, Production of doubly charged scalars from the decay of singly charged scalars in the Higgs triplet model, Phys. Rev. D **84**, 035010 (2011).

[22] F. Arbabifar, S. Bahrami, and M. Frank, Neutral Higgs bosons in the Higgs triplet model with nontrivial mixing, Phys. Rev. D **87**, 015020 (2013).
[23] C.-W. Chiang, T. Nomura, and K. Tsumura, Search for doubly charged Higgs bosons using the same-sign diboson mode at the LHC, Phys. Rev. D **85**, 095023 (2012).
[24] A. G. Akeroyd, S. Moretti, and H. Sugiyama, Five-lepton and six-lepton signatures from production of neutral triplet scalars in the Higgs triplet model, Phys. Rev. D **85**, 055026 (2012).
[25] E. J. Chun and P. Sharma, Same-sign tetra-leptons from type II seesaw, J. High Energy Phys. 08 (2012) 162.
[26] F. del Águila and M. Chala, LHC bounds on lepton number violation mediated by doubly and singly-charged scalars, J. High Energy Phys. 03 (2014) 027.
[27] E. J. Chun and P. Sharma, Search for a doubly-charged boson in four lepton final states in type II seesaw, Phys. Lett. B **728**, 256 (2014).
[28] S. Kanemura, K. Yagyu, and H. Yokoya, First constraint on the mass of doubly-charged Higgs bosons in the same-sign diboson decay scenario at the LHC, Phys. Lett. B **726**, 316 (2013).
[29] P. S. Bhupal Dev, D. K. Ghosh, N. Okada, and I. Saha, 125 GeV Higgs boson and the type-II seesaw model, J. High Energy Phys. 03 (2013) 150; 05 (2013) 49(E).
[30] S. Kanemura, M. Kikuchi, K. Yagyu, and H. Yokoya, Bounds on the mass of doubly-charged Higgs bosons in the same-sign diboson decay scenario, Phys. Rev. D **90**, 115018 (2014).
[31] S. Kanemura, M. Kikuchi, H. Yokoya, and K. Yagyu, LHC Run-I constraint on the mass of doubly charged Higgs bosons in the same-sign diboson decay scenario, Prog. Theor. Exp. Phys. **2015**, 051B02 (2015).
[32] Z. Kang, J. Li, T. Li, Y. Liu, and G.-Z. Ning, Light doubly charged Higgs boson via the WW^* channel at LHC, Eur. Phys. J. C **75**, 574 (2015).
[33] Z.-L. Han, R. Ding, and Y. Liao, LHC phenomenology of type II seesaw: Nondegenerate case, Phys. Rev. D **91**, 093006 (2015).
[34] Z.-L. Han, R. Ding, and Y. Liao, LHC phenomenology of the type II seesaw mechanism: Observability of neutral scalars in the nondegenerate case, Phys. Rev. D **92**, 033014 (2015).
[35] M. Mitra, S. Niyogi, and M. Spannowsky, Type-II seesaw model and multilepton signatures at hadron colliders, Phys. Rev. D **95**, 035042 (2017).
[36] D. K. Ghosh, N. Ghosh, I. Saha, and A. Shaw, Revisiting the high-scale validity of the type II seesaw model with novel LHC signature, Phys. Rev. D **97**, 115022 (2018).
[37] S. Antusch, O. Fischer, A. Hammad, and C. Scherb, Low scale type II seesaw: Present constraints and prospects for displaced vertex searches, J. High Energy Phys. 02 (2019) 157.
[38] P. S. Bhupal Dev and Y. Zhang, Displaced vertex signatures of doubly charged scalars in the type-II seesaw and its left-right extensions, J. High Energy Phys. 10 (2018) 199.
[39] T. B. de Melo, F. S. Queiroz, and Y. Villamizar, Doubly charged scalar at the high-luminosity and high-energy LHC, Int. J. Mod. Phys. A **34**, 1950157 (2019).
[40] R. Primulando, J. Julio, and P. Uttayarat, Scalar phenomenology in type-II seesaw model, J. High Energy Phys. 08 (2019) 024.
[41] E. J. Chun, S. Khan, S. Mandal, M. Mitra, and S. Shil, Same-sign tetralepton signature at the large hadron collider and a future pp collider, Phys. Rev. D **101**, 075008 (2020).
[42] R. Padhan, D. Das, M. Mitra, and A. Kumar Nayak, Probing doubly and singly charged Higgs bosons at the pp collider HE-LHC, Phys. Rev. D **101**, 075050 (2020).
[43] J. Gluza, M. Kordiaczynska, and T. Srivastava, Discriminating the HTM and MLRSM models in collider studies via doubly charged Higgs boson pair production and the subsequent leptonic decays, Chin. Phys. C **45**, 073113 (2021).
[44] S. Ashanujjaman and K. Ghosh, Revisiting type-II seesaw: Present limits and future prospects at LHC, J. High Energy Phys. 03 (2022) 195.
[45] S. Ashanujjaman, K. Ghosh, and R. Sahu, Low-mass doubly charged Higgs bosons at the LHC, Phys. Rev. D **107**, 015018 (2023).
[46] R. Ruiz, Doubly charged Higgs boson production at hadron colliders II: A Zee-Babu case study, J. High Energy Phys. 10 (2022) 200.
[47] J. Butterworth, J. Heeck, S. H. Jeon, O. Mattelaer, and R. Ruiz, Testing the scalar triplet solution to CDF's heavy W problem at the LHC, Phys. Rev. D **107**, 075020 (2023).
[48] W. Rodejohann and H. Zhang, Higgs triplets at like-sign linear colliders and neutrino mixing, Phys. Rev. D **83**, 073005 (2011).
[49] S. Blunier, G. Cottin, M. A. Díaz, and B. Koch, Phenomenology of a Higgs triplet model at future e^+e^- colliders, Phys. Rev. D **95**, 075038 (2017).
[50] T. Nomura, H. Okada, and H. Yokoya, Discriminating leptonic Yukawa interactions with doubly charged scalar at the ILC, Nucl. Phys. **B929**, 193 (2018).
[51] A. Crivellin, M. Ghezzi, L. Panizzi, G. M. Pruna, and A. Signer, Low- and high-energy phenomenology of a doubly charged scalar, Phys. Rev. D **99**, 035004 (2019).
[52] P. Agrawal, M. Mitra, S. Niyogi, S. Shil, and M. Spannowsky, Probing the type-II seesaw mechanism through the production of Higgs bosons at a lepton collider, Phys. Rev. D **98**, 015024 (2018).
[53] L. Rahili, A. Arhrib, and R. Benbrik, Associated production of SM Higgs with a photon in type-II seesaw models at the ILC, Eur. Phys. J. C **79**, 940 (2019).
[54] P. Bandyopadhyay, A. Karan, and C. Sen, Discerning signatures of seesaw models and complementarity of leptonic colliders, arXiv:2011.04191.
[55] S. Ashanujjaman, K. Ghosh, and K. Huitu, Type-II seesaw: Searching the LHC elusive low-mass triplet-like Higgses at e^-e^+ colliders, Phys. Rev. D **106**, 075028 (2022).
[56] A. Das, S. Mandal, and S. Shil, Testing electroweak scale seesaw models at $e^-\gamma$ and $\gamma\gamma$ colliders, arXiv:2304.06298.
[57] W. Rodejohann, Inverse neutrino-less double beta decay revisited: Neutrinos, Higgs triplets and a muon collider, Phys. Rev. D **81**, 114001 (2010).
[58] T. Li, C.-Y. Yao, and M. Yuan, Revealing the origin of neutrino masses through the type II seesaw mechanism at

high-energy muon colliders, J. High Energy Phys. 03 (2023) 137.
[59] S. P. Maharathy and M. Mitra, Type-II see-saw at $\mu^+\mu^-$ collider, arXiv:2304.08732.
[60] K. Fridell, R. Kitano, and R. Takai, Lepton flavor physics at $\mu^+\mu^+$ colliders, arXiv:2304.14020.
[61] P. S. B. Dev, S. Khan, M. Mitra, and S. K. Rai, Doubly-charged Higgs boson at a future electron-proton collider, Phys. Rev. D **99**, 115015 (2019).
[62] X.-H. Yang and Z.-J. Yang, Doubly charged Higgs production at future ep colliders, Chin. Phys. C **46**, 063107 (2022).
[63] F. F. Deppisch, P. S. Bhupal Dev, and A. Pilaftsis, Neutrinos and collider physics, New J. Phys. **17**, 075019 (2015).
[64] Y. Cai, T. Han, T. Li, and R. Ruiz, Lepton number violation: Seesaw models and their collider tests, Front. Phys. **6**, 40 (2018).
[65] E. J. Chun, K. Y. Lee, and S. C. Park, Testing Higgs triplet model and neutrino mass patterns, Phys. Lett. B **566**, 142 (2003).
[66] M. Kadastik, M. Raidal, and L. Rebane, Direct determination of neutrino mass parameters at future colliders, Phys. Rev. D **77**, 115023 (2008).
[67] A. Arhrib, R. Benbrik, M. Chabab, G. Moultaka, M. C. Peyranere, L. Rahili, and J. Ramadan, The Higgs potential in the type II seesaw model, Phys. Rev. D **84**, 095005 (2011).
[68] E. J. Chun, H. M. Lee, and P. Sharma, Vacuum stability, perturbativity, EWPD and Higgs-to-diphoton rate in type II seesaw models, J. High Energy Phys. 11 (2012) 106.
[69] D. Das and A. Santamaria, Updated scalar sector constraints in the Higgs triplet model, Phys. Rev. D **94**, 015015 (2016).
[70] J. Heeck, W-boson mass in the triplet seesaw model, Phys. Rev. D **106**, 015004 (2022).
[71] G. Aad *et al.* (ATLAS Collaboration), Search for doubly-charged Higgs bosons in like-sign dilepton final states at $\sqrt{s} = 7$ TeV with the ATLAS detector, Eur. Phys. J. C **72**, 2244 (2012).
[72] S. Chatrchyan *et al.* (CMS Collaboration), A search for a doubly-charged Higgs boson in pp collisions at $\sqrt{s} = 7$ TeV, Eur. Phys. J. C **72**, 2189 (2012).
[73] G. Aad *et al.* (ATLAS Collaboration), Search for anomalous production of prompt same-sign lepton pairs and pair-produced doubly charged Higgs bosons with $\sqrt{s} = 8$ TeV pp collisions using the ATLAS detector, J. High Energy Phys. 03 (2015) 041.
[74] V. Khachatryan *et al.* (CMS Collaboration), Study of Vector Boson Scattering and Search for New Physics in Events with Two Same-Sign Leptons and Two Jets, Phys. Rev. Lett. **114**, 051801 (2015).
[75] CMS Collaboration, Search for a doubly-charged Higgs boson with $\sqrt{s} = 8$ TeV pp collisions at the CMS experiment, Report No. CMS-PAS-HIG-14-039, 2016, http://cds.cern.ch/record/2127498.
[76] CMS Collaboration, A search for doubly-charged Higgs boson production in three and four lepton final states at $\sqrt{s} = 13$ TeV, Report No. CMS-PAS-HIG-16-036, 2017, https://cds.cern.ch/record/2242956.
[77] M. Aaboud *et al.* (ATLAS Collaboration), Search for doubly charged Higgs boson production in multi-lepton final states with the ATLAS detector using proton–proton collisions at $\sqrt{s} = 13$ TeV, Eur. Phys. J. C **78**, 199 (2018).
[78] A. M. Sirunyan *et al.* (CMS Collaboration), Observation of Electroweak Production of Same-Sign W Boson Pairs in the Two Jet and Two Same-Sign Lepton Final State in Proton-Proton Collisions at $\sqrt{s} = 13$ TeV, Phys. Rev. Lett. **120**, 081801 (2018).
[79] M. Aaboud *et al.* (ATLAS Collaboration), Search for doubly charged scalar bosons decaying into same-sign W boson pairs with the ATLAS detector, Eur. Phys. J. C **79**, 58 (2019).
[80] G. Aad *et al.* (ATLAS Collaboration), Search for doubly and singly charged Higgs bosons decaying into vector bosons in multi-lepton final states with the ATLAS detector using proton-proton collisions at $\sqrt{s} = 13$ TeV, J. High Energy Phys. 06 (2021) 146.
[81] G. Aad *et al.* (ATLAS Collaboration), Search for doubly and singly charged Higgs bosons decaying into vector bosons in multi-lepton final states with the ATLAS detector using proton-proton collisions at $\sqrt{s} = 13$ TeV, J. High Energy Phys. 06 (2021) 146.
[82] ATLAS Collaboration, Search for doubly charged Higgs boson production in multi-lepton final states using 139 fb^{-1} of proton–proton collisions at $\sqrt{s} = 13$ TeV with the ATLAS detector, Report No. CERN-EP-2022-212, 2022.
[83] G. Aad *et al.* (ATLAS Collaboration), Search for new phenomena in events with an energetic jet and missing transverse momentum in pp collisions at $\sqrt{s} = 13$ TeV with the ATLAS detector, Phys. Rev. D **103**, 112006 (2021).
[84] A. Tumasyan *et al.* (CMS Collaboration), Search for new particles in events with energetic jets and large missing transverse momentum in proton-proton collisions at $\sqrt{s} = 13$ TeV, J. High Energy Phys. 11 (2021) 153.
[85] G. Aad *et al.* (ATLAS Collaboration), Searches for electroweak production of supersymmetric particles with compressed mass spectra in $\sqrt{s} = 13$ TeV pp collisions with the ATLAS detector, Phys. Rev. D **101**, 052005 (2020).
[86] A. Tumasyan *et al.* (CMS Collaboration), Search for supersymmetry in final states with two or three soft leptons and missing transverse momentum in proton-proton collisions at $\sqrt{s} = 13$ TeV, J. High Energy Phys. 04 (2022) 091.
[87] F. Staub, SARAH 4: A tool for (not only SUSY) model builders, Comput. Phys. Commun. **185**, 1773 (2014).
[88] F. Staub, Exploring new models in all detail with SARAH, Adv. High Energy Phys. **2015**, 840780 (2015).
[89] C. Degrande, C. Duhr, B. Fuks, D. Grellscheid, O. Mattelaer, and T. Reiter, UFO—The universal FeynRules output, Comput. Phys. Commun. **183**, 1201 (2012).
[90] J. Alwall, M. Herquet, F. Maltoni, O. Mattelaer, and T. Stelzer, MadGraph 5: Going beyond, J. High Energy Phys. 06 (2011) 128.
[91] J. Alwall, R. Frederix, S. Frixione, V. Hirschi, F. Maltoni, O. Mattelaer, H. S. Shao, T. Stelzer, P. Torrielli, and M. Zaro, The automated computation of tree-level and next-to-leading order differential cross sections, and their

matching to parton shower simulations, J. High Energy Phys. 07 (2014) 079.
[92] R. D. Ball, V. Bertone, S. Carrazza, L. Del Debbio, S. Forte, A. Guffanti, N. P. Hartland, and J. Rojo (NNPDF Collaboration), Parton distributions with QED corrections, Nucl. Phys. **B877**, 290 (2013).
[93] R. D. Ball *et al.* (NNPDF Collaboration), Parton distributions for the LHC Run II, J. High Energy Phys. 04 (2015) 040.
[94] B. Fuks, M. Nemevšek, and R. Ruiz, Doubly charged Higgs boson production at hadron colliders, Phys. Rev. D **101**, 075022 (2020).
[95] T. Sjöstrand, S. Ask, J. R. Christiansen, R. Corke, N. Desai, P. Ilten, S. Mrenna, S. Prestel, C. O. Rasmussen, and P. Z. Skands, An introduction to PYTHIA 8.2, Comput. Phys. Commun. **191**, 159 (2015).
[96] S. Catani, L. Cieri, G. Ferrera, D. de Florian, and M. Grazzini, Vector Boson Production at Hadron Colliders: A Fully Exclusive QCD Calculation at NNLO, Phys. Rev. Lett. **103**, 082001 (2009).
[97] G. Balossini, G. Montagna, C. M. Carloni Calame, M. Moretti, O. Nicrosini, F. Piccinini, M. Treccani, and A. Vicini, Combination of electroweak and QCD corrections to single W production at the Fermilab Tevatron and the CERN LHC, J. High Energy Phys. 01 (2010) 013.
[98] J. M. Campbell, R. K. Ellis, and C. Williams, Vector boson pair production at the LHC, J. High Energy Phys. 07 (2011) 018.
[99] F. Cascioli, T. Gehrmann, M. Grazzini, S. Kallweit, P. Maierhöfer, A. von Manteuffel, S. Pozzorini, D. Rathlev, L. Tancredi, and E. Weihs, ZZ production at hadron colliders in NNLO QCD, Phys. Lett. B **735**, 311 (2014).
[100] J. M. Campbell, R. K. Ellis, and C. Williams, Associated production of a Higgs boson at NNLO, J. High Energy Phys. 06 (2016) 179.
[101] D. de Florian *et al.* (LHC Higgs Cross Section Working Group), Handbook of LHC Higgs cross sections: 4. Deciphering the nature of the Higgs sector, 10.23731/CYRM-2017-002 (2016).
[102] Y.-B. Shen, R.-Y. Zhang, W.-G. Ma, X.-Z. Li, and L. Guo, NLO QCD and electroweak corrections to WWW production at the LHC, Phys. Rev. D **95**, 073005 (2017).
[103] D. T. Nhung, L. D. Ninh, and M. M. Weber, NLO corrections to WWZ production at the LHC, J. High Energy Phys. 12 (2013) 096.
[104] Y.-B. Shen, R.-Y. Zhang, W.-G. Ma, X.-Z. Li, Y. Zhang, and L. Guo, NLO QCD + NLO EW corrections to WZZ productions with leptonic decays at the LHC, J. High Energy Phys. 10 (2015) 186; 10 (2016) 156(E).
[105] H. Wang, R.-Y. Zhang, W.-G. Ma, L. Guo, X.-Z. Li, and S.-M. Wang, NLO QCD + EW corrections to ZZZ production with subsequent leptonic decays at the LHC, J. Phys. G **43**, 115001 (2016).
[106] R. Frederix, S. Frixione, V. Hirschi, F. Maltoni, O. Mattelaer, P. Torrielli, E. Vryonidou, and M. Zaro, Higgs pair production at the LHC with NLO and parton-shower effects, Phys. Lett. B **732**, 142 (2014).
[107] N. Kidonakis, Theoretical results for electroweak-boson and single-top production, Proc. Sci. DIS2015 (**2015**) 170 [arXiv:1506.04072].
[108] C. Muselli, M. Bonvini, S. Forte, S. Marzani, and G. Ridolfi, Top quark pair production beyond NNLO, J. High Energy Phys. 08 (2015) 076.
[109] A. Broggio, A. Ferroglia, R. Frederix, D. Pagani, B. D. Pecjak, and I. Tsinikos, Top-quark pair hadroproduction in association with a heavy boson at NLO + NNLL including EW corrections, J. High Energy Phys. 08 (2019) 039.
[110] R. Frederix, D. Pagani, and M. Zaro, Large NLO corrections in $t\bar{t}W^{\pm}$ and $t\bar{t}t\bar{t}$ hadroproduction from supposedly subleading EW contributions, J. High Energy Phys. 02 (2018) 031.
[111] ATLAS Collaboration, Electron efficiency measurements with the ATLAS detector using the 2015 LHC proton-proton collision data, Report No. ATLAS-CONF-2016-024, 2016.
[112] M. Aaboud *et al.* (ATLAS Collaboration), Search for doubly charged Higgs boson production in multilepton final states with the ATLAS detector using proton–proton collisions at $\sqrt{s} = 13$ TeV, Eur. Phys. J. C **78**, 199 (2018).
[113] J. de Favereau, C. Delaere, P. Demin, A. Giammanco, V. Lemaître, A. Mertens, and M. Selvaggi (DELPHES 3 Collaboration), DELPHES 3, A modular framework for fast simulation of a generic collider experiment, J. High Energy Phys. 02 (2014) 057.
[114] M. Cacciari, G. P. Salam, and G. Soyez, The anti-k_t jet clustering algorithm, J. High Energy Phys. 04 (2008) 063.
[115] M. Cacciari, G. P. Salam, and G. Soyez, FastJet user manual, Eur. Phys. J. C **72**, 1896 (2012).
[116] M. Aaboud *et al.* (ATLAS Collaboration), Performance of the ATLAS trigger system in 2015, Eur. Phys. J. C **77**, 317 (2017).
[117] G. Aad *et al.* (ATLAS Collaboration), Performance of electron and photon triggers in ATLAS during LHC Run 2, Eur. Phys. J. C **80**, 47 (2020).
[118] A. M. Sirunyan *et al.* (CMS Collaboration), Performance of the CMS Level-1 trigger in proton-proton collisions at $\sqrt{s} = 13$ TeV, J. Instrum. **15**, P10017 (2020).
[119] A. Hocker *et al.*, TMVA—Toolkit for multivariate data analysis, arXiv:physics/0703039.
[120] R. Brun, F. Rademakers, and S. Panacek, ROOT, An object oriented data analysis framework, in *Proceedings of the CERN School of Computing (CSC 2000)* (CERN, Geneva, 2000), pp. 11–42.
[121] G. Cowan, K. Cranmer, E. Gross, and O. Vitells, Asymptotic formulae for likelihood-based tests of new physics, Eur. Phys. J. C **71**, 1554 (2011); **73**, 2501(E) (2013).
[122] T. P. Li and Y. Q. Ma, Analysis methods for results in gamma-ray astronomy, Astrophys. J. **272**, 317 (1983).
[123] R. D. Cousins, J. T. Linnemann, and J. Tucker, Evaluation of three methods for calculating statistical significance when incorporating a systematic uncertainty into a test of the background-only hypothesis for a Poisson process, Nucl. Instrum. Methods Phys. Res., Sect. A **595**, 480 (2008).